Mapping the sites of the lipoprotein lipase (LPL)–angiopoietin-like protein 4 (ANGPTL4) interaction provides mechanistic insight into LPL inhibition

Received for publication, September 28, 2018, and in revised form, December 21, 2018 Published, Papers in Press, December 27, 2018, DOI 10.1074/jbc.RA118.005932

Aspen R. Gutgsell[‡], Swapnil V. Ghodge[§], Albert A. Bowers[§], and Saskia B. Neher[‡1]

From the [‡]Department of Biochemistry and Biophysics, University of North Carolina at Chapel Hill, Chapel Hill, North Carolina 27599 and the [§]Division of Chemical Biology and Medicinal Chemistry, Eshelman School of Pharmacy, University of North Carolina at Chapel Hill, Chapel Hill, North Carolina 27599

Edited by George M. Carman

Cardiovascular disease has been the leading cause of death throughout the world for nearly 2 decades. Hypertriglyceridemia affects more than one-third of the population in the United States and is an independent risk factor for cardiovascular disease. Despite the frequency of hypertriglyceridemia, treatment options are primarily limited to diet and exercise. Lipoprotein lipase (LPL) is an enzyme responsible for clearing triglycerides from circulation, and its activity alone can directly control plasma triglyceride concentrations. Therefore, LPL is a good target for triglyceride-lowering therapeutics. One approach for treating hypertriglyceridemia may be to increase the amount of enzymatically active LPL by preventing its inhibition by angiopoietin-like protein 4 (ANGPTL4). However, little is known about how these two proteins interact. Therefore, we used hydrogen–deuterium exchange MS to identify potential binding sites between LPL and ANGPTL4. We validated sites predicted to be located at the protein–protein interface by using chimeric variants of LPL and an LPL peptide mimetic. We found that ANGPTL4 binds LPL near the active site at the lid domain and a nearby α-helix. Lipase lid domains cover the active site to control both enzyme activation and substrate specificity. Our findings suggest that ANGPTL4 specifically inhibits LPL by binding the lid domain, which could prevent substrate catalysis at the active site. The structural details of the LPL–ANGPTL4 interaction uncovered here may inform the development of therapeutics targeted to disrupt this interaction for the management of hypertriglyceridemia.

Lipoprotein lipase (LPL)[2] is a key enzyme for regulating plasma triglyceride levels (1, 2). LPL hydrolyzes triglycerides contained within lipoprotein particles in the capillary endothelium to facilitate the passage of free fatty acids into surrounding tissues (3, 4). Patients with loss-of-function mutations in LPL have extremely high levels of plasma triglycerides, or hypertriglyceridemia, that can cause complications such as pancreatitis, eruptive xanthomas, and lipemia retinalis (5). Although LPL deficiency is rare, moderate hypertriglyceridemia is common with more than three million cases diagnosed every year in the United States (6). Despite the frequency of hypertriglyceridemia, treatment options are limited to diet and exercise, statins, or fibrates (7). Historically, the development of novel triglyceride-lowering therapeutics was curbed due to inconclusive epidemiological associations between hypertriglyceridemia and cardiovascular risk (8, 9). However, recent genetic studies have demonstrated that hypertriglyceridemia is an independent risk factor for cardiovascular disease and should be addressed in the clinic (10–12).

LPL is first synthesized in the parenchymal cells of heart, skeletal muscle, and adipose tissue. LPL is then secreted and transported to the vascular endothelium where it is anchored to the walls of the vessel lumen (13). Here, LPL is regulated by activators and inhibitors to precisely control the delivery of free fatty acids to either oxidative tissues for catabolism or adipose tissue for storage (1, 14–16). One family of inhibitory proteins, known as angiopoietin-like proteins (ANGPTL3, -4, and -8), are up-regulated in response to nutritional cues to inhibit LPL in a tissue-specific manner (17). ANGPTL8 is up-regulated in the postprandial state and interacts with ANGPTL3 to cooperatively inhibit LPL within oxidative tissues (17). Inhibition of LPL in oxidative tissues, while simultaneously leaving LPL active in adipose tissue, directs free fatty acids to adipose tissue for storage (15). Conversely, in the fasted state ANGPTL4 is up-regulated to inhibit LPL in the adipose tissue (18). Inhibition of LPL in adipose tissue, while simultaneously leaving LPL active in oxidative tissue, directs free fatty acids to these tissues for catabolism (15).

Human genome-wide association studies have identified individuals with loss-of-function mutations in either ANGPTL3 or ANGPTL4 as having a unique lipid profile that significantly

This work was supported by National Institutes of Health Grants R01HL125654 (to S. B. N.) and R35GM125005 (to A. A. B.). The authors declare that they have no conflicts of interest with the contents of this article. The content is solely the responsibility of the authors and does not necessarily represent the official views of the National Institutes of Health. This article contains Figs. S1–S5, Table S1, and Refs. 1–2.

[1] To whom correspondence should be addressed: Dept. of Biochemistry and Biophysics, University of North Carolina at Chapel Hill, 120 Mason Farm Rd., CB7260, Chapel Hill, NC 27599. Tel.: 919-966-9550; Fax: 919-966-2852; E-mail: neher@email.unc.edu.

[2] The abbreviations used are: LPL, lipoprotein lipase; bLPL, bovine LPL; bis-tris, 2-[bis(2-hydroxyethyl)amino]-2-(hydroxymethyl)propane-1,3-diol; Fmoc, *N*-(9-fluorenyl)methoxycarbonyl; DMF, *N*,*N*-dimethylformamide; NEM, *N*-ethylmaleimide; TCEP, tris(2-carboxyethyl)phosphine; DGGR, 1,2-di-*O*-lauryl-*rac*-glycero-3-(glutaric acid 6-methylresofurin ester); TAMRA, tetramethylrhodamine; HDX-MS, hydrogen–deuterium exchange MS; HL, hepatic lipase; ITC, isothermal calorimetry; LDL, low-density lipoprotein; HDL, high density lipoprotein.

decreases their risk for developing cardiovascular disease (19–21). Loss-of-function mutations in ANGPTL3 results in hypobetalipoproteinemia-2, which is characterized by low levels of plasma triglycerides, HDL, and LDL cholesterol (22, 23). Individuals with hypobetalipoproteinemia-2 appear to have few negative health effects and have motivated the development of novel antisense oligonucleotide therapeutics that silence ANGPTL3 expression (22, 24). By comparison, inactivating mutations in ANGPTL4 result in a slightly different lipid profile with low levels of plasma triglycerides, high levels of HDL cholesterol, and no apparent effect on LDL cholesterol (19, 25, 26). Previous studies using either antibody to silence ANGPTL4 in monkeys or the genetic loss of ANGPTL4 in mice recapitulate low levels of plasma triglycerides seen in humans with loss-of-function ANGPTL4 mutations (25, 27). However, both ANGPTL4 knockdown monkeys and knockout mice inexplicably developed severe mesenteric lymphadenitis, or inflammation in the abdominal lymph nodes, when placed on a high-fat diet (25, 27, 28). Individuals with loss-of-function mutations in ANGPTL4 do not have increased rates of lymphadenopathy, and the animals do not develop this phenotype on standard chow or low-fat diets (25, 26).

ANGPTL4 was originally thought to be an adipokine given its robust expression in adipocytes and hepatocytes, but it has since been reclassified with roles in angiogenesis, wound repair, kidney function, tumorigenesis, redox regulation, and energy homeostasis (29). Structurally, ANGPTL4 is composed of a coiled-coil N-terminal domain and a C-terminal fibrinogen-like domain that is selectively cleaved by proprotein convertases in certain tissues (30, 31). Adipocytes primarily secrete full-length ANGPTL4, and hepatocytes secrete the cleaved N- and C-terminal domains (29, 32). The N-terminal domain, herein referred to as nANGPTL4, is known to potently inhibit LPL, whereas the C-terminal domain is thought to be involved in other roles like angiogenesis or wound repair (33–35). Given the diverse roles for ANGPTL4, it is not surprising that complete silencing results in a severe diet-induced pathology (29, 36). The disparity between an advantageous phenotype in human variants and a pathological phenotype in animals suggests additional research is needed to understand the precise function of each ANGPTL4 species.

We set out to characterize how nANGPTL4 binds LPL and use this information to block the interaction using a small peptide mimetic of an LPL-binding site. Using both hydrogen–deuterium exchange MS (HDX-MS) and site-specific mutagenesis, we determined that nANGPTL4 binds near the active site of LPL at the lid domain (residues 224–238) and a nearby α-helix (residues 89–102). Moreover, a peptide mimetic of the LPL lid domain is capable of binding nANGPTL4 and protects full-length LPL from inhibition. Our data suggest nANGPTL4 reversibly inhibits LPL by binding the lid domain to prevent substrate catalysis by the active site.

Results

Hydrogen–deuterium exchange MS reveals four nANGPTL4-binding sites on bovine LPL

To answer the question of how nANGPTL4 mediates inhibition of LPL, we used HDX-MS to identify residues at the interface of this protein–protein interaction. The rate of deuterium exchange between amide hydrogens is used to probe protein secondary structure and allosteric conformational changes induced by binding interactions (37, 38). We performed HDX-MS on bovine LPL (bLPL) alone, nANGPTL4 alone, and a combination of bLPL and nANGPTL4. Samples were incubated in deuterated buffer for 0, 1, 5, and 10 min, quenched, and digested for immediate analysis by reverse-phase chromatography coupled to MS. Between bLPL and nANGPTL4, we identified 710 unique peptides (Table S1).

The difference in deuterium uptake for bLPL was measured under −nANGPTL4 and +nANGPTL4 conditions and is represented using a heat map to highlight areas with decreased exchange (*dark blue*) and increased exchange (*red*) (Fig. 1*A*). Peptide sequences that were statistically significantly different (p value < 0.05) between the −nANGPTL4 and +nANGPTL4 conditions are represented with percent deuterium uptake curves (Fig. 1*A*) and colored based on differential deuterium exchange on a computational model of LPL generated by Hayne *et al.* (original model, see Ref. 39) (Fig. 1*B*). Because the crystal structure of LPL is not known, we have also included two additional computational models of LPL generated by Hayne *et al.* (39) in Fig. S1, *A* and *B*. A decrease in deuterium exchange in the complex condition suggests that those peptide sequences are at the binding interface. We identified four potential nANGPTL4-binding sites on bLPL at residues 17–26, 89–102, 224–238, and 290–311 (residue 1 is the first amino acid after signal peptide cleavage, Fig. 1, *A* and *B*). Herein, these sites will be referred to as the N-terminal β-turn, lid-proximal helix, lid, and the furin cleavage region, respectively. Interestingly, there were several sites within bLPL that increased in exchange: residues 63–72, 75–83, 103–113, 133–146, and 166–180 (after signal peptide cleavage) (Fig. S1*C*). Regions of increased deuterium exchange correspond to more structurally dynamic regions (38). It is unclear at this time whether regions with increased deuterium exchange result from bLPL unfolding as suggested by Mysling *et al.* (40) or other causes, such as allosteric changes (38, 41).

To address the possibility of nANGPTL4-mediated irreversible unfolding of bLPL, we utilized a kinetic assay. Reversible, noncompetitive inhibition can be distinguished from irreversible inactivation by measuring bLPL activity at different concentrations under V_{max} conditions in the presence and absence of nANGPTL4. By plotting V_{max} *versus* the total concentration of bLPL, the data fit a linear equation with the slope equal to the k_{cat} ($V_{max} = k_{cat}[E_{total}]$, where $[E_{total}]$ is the total enzyme concentration) (42). For a reversible, noncompetitive inhibitor, both the uninhibited and inhibited conditions intersect the origin, and the slope of the inhibited condition is less than the uninhibited control by the quantity $1 + ([I]/(K_i)$, where [I] is the concentration of inhibitor and K_i is the inhibition constant (Fig. S2*A*). For an irreversible inhibitor, the slope of the inhibited condition is the same as the uninhibited control. However, the line does not intersect the x axis at the origin, but rather at a position on the x axis that is equivalent to the amount of enzyme that is irreversibly inactivated (Fig. S2*B*). Plotting V_{max} *versus* the total concentration of active bLPL shows that both the inhibited and control conditions intersect the origin (Fig. S2*C*). Additionally, the slope of the inhibited plot decreased

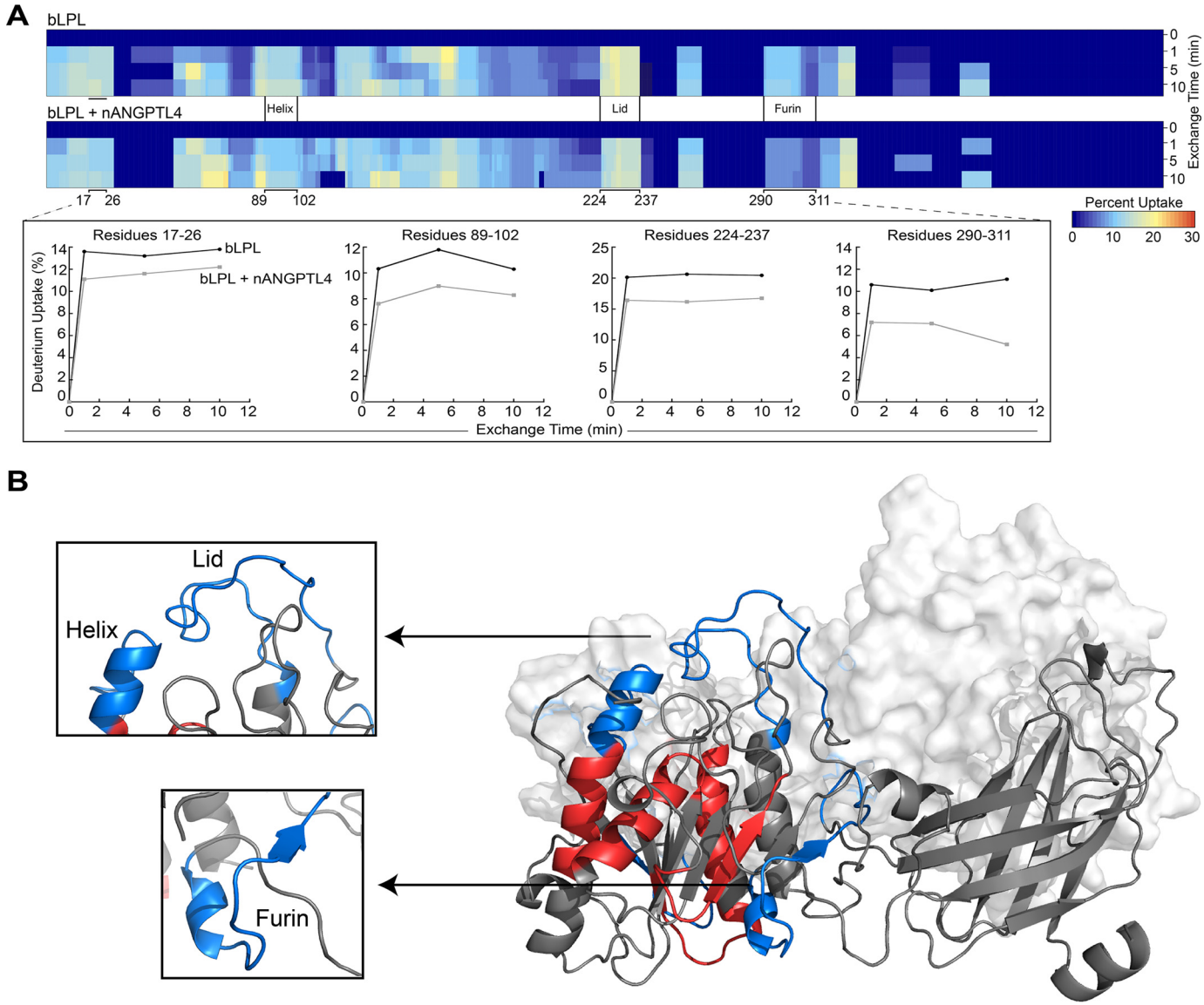

Figure 1. Decreased deuterium exchange suggests four potential binding sites on bLPL. Sites of deuterium exchange were identified using LC-MS-MS after incubation of bLPL, nANGPTL4, or a combination of bLPL and nANGPTL4 in 99.9% deuterated solution for 0, 1, 5, and 10 min. *A,* heat maps were generated using percent deuterium uptake values for all peptides with a standard deviation of less than 0.2 Da. Deuterium uptake curves are shown for peptides that were statistically significantly different between the bLPL apo (*black*) and complex state (*gray*) at each time point. Sites of differential deuterium exchange were determined using unpaired two-tailed Student's *t* test with cutoff of $p < 0.05$. *B,* computational model of dimeric LPL generated by Hayne *et al.* (Original model, see Ref. 39). Peptide sequences with differential deuterium exchange in the complex state at every time point are colored *blue* for decreased exchange and *red* for increased exchange. For simplicity, one monomer unit is represented as a cartoon model (*gray*), and the other unit is a surface model (*white*). Panels are zoomed in on the lid-proximal helix, lid, and furin cleavage region (*blue*).

from 1.097 to 0.541. These plots indicate reversible, noncompetitive inhibition (Fig. S2*A*).

We identified two sites with decreased deuterium exchange in nANGPTL4: residues 15–33 and 95–106 (after signal peptide cleavage) (Fig. 2). Residues 15–33 are in agreement with previous reports detailing a peptide sequence necessary for nANGPTL4 inhibition of LPL, and site 95–106 has not been previously reported (34, 35). There were no sites on nANGPTL4 that increased in deuterium exchange in the presence of bLPL.

Human LPL_{HL} chimeric molecules are insensitive to inhibition by nANGPTL4

To validate potential nANGPTL4-binding sites on LPL, we mutagenized human LPL in regions with decreased deuterium exchange and screened for nANGPTL4 inhibition *in vitro* (Fig. 3). LPL shares 44% sequence identity with hepatic lipase (HL), which has been putatively shown to be resistant to ANGPTL4 inhibition, although the data surrounding this issue have been contradictory (43–45). Here, we show that HL is not inhibited by nANGPTL4, even at a 1:4000 molar excess (Figs. 4*B* and 5*A*). Therefore, we used the corresponding HL sequences to generate LPL_{HL} chimeras in two regions near the active site: the lid-proximal helix and the lid (Fig. 3). Previous studies have shown that the lipase lids alone dictate substrate specificity, and the chimeric lid mutants of LPL, HL, and endothelial lipase alter both substrate specificity and enzyme kinetics (46–48). If nANGPTL4 binds the lid of LPL, it could explain why ANGPTL4 specifically inhibits LPL

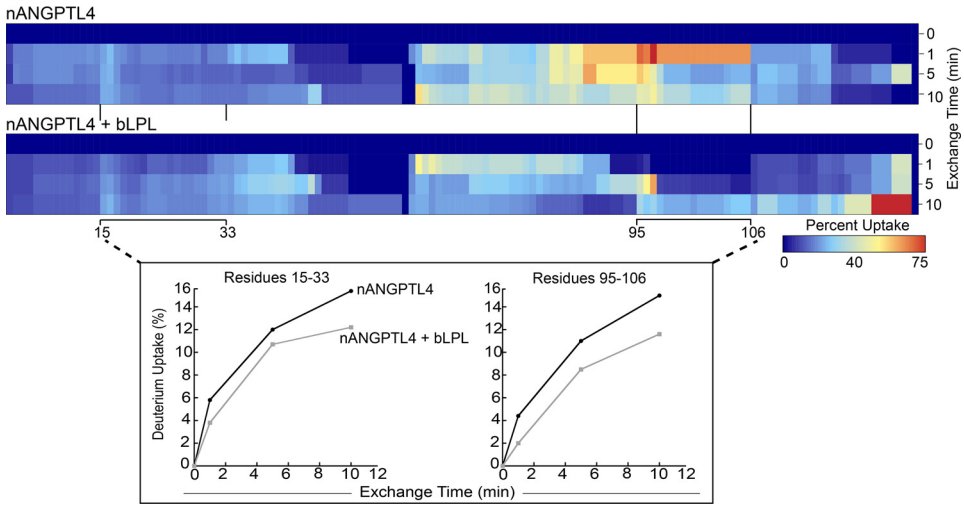

Figure 2. Decreased deuterium exchange suggests two potential binding sites on nANGPTL4. Heat maps of nANGPTL4 and nANGPTL4 + bLPL were generated using percent deuterium uptake values for peptide sequences with a standard deviation of less than 0.2 Da. Percent uptake curves were generated for sites that were statistically significantly different between the nANGPTL4 apo and complex state. Sites of differential deuterium exchange were determined using unpaired two-tailed Student's *t* test with cutoff of $p < 0.05$.

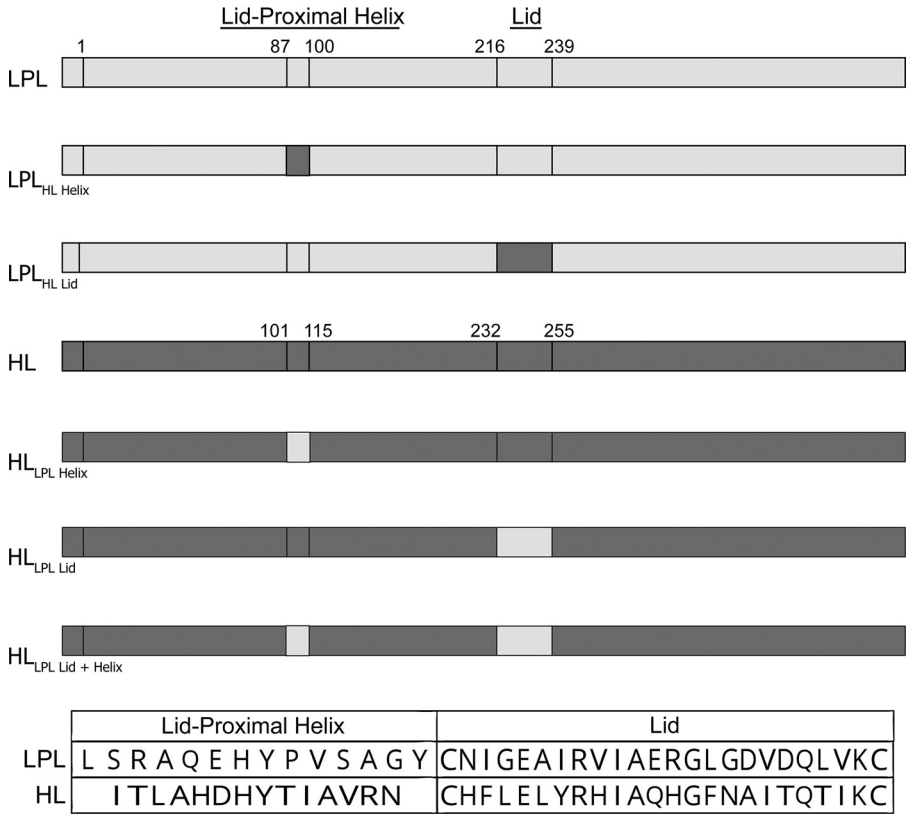

Figure 3. Human LPL and HL construct schematic. LPL (*light gray*) and HL (*dark gray*) sequences were aligned and defined according to potential nANGPTL4-binding sites identified by our HDX-MS experiments using bLPL. The corresponding sequences in human LPL and HL are defined as the lid-proximal helix (residues 87–100 or 101–115) or the lid (residues 216–239 or 232–255). Chimeric mutants were generated using overlap extension PCR.

rather than HL, as these lid sequences have only 32% identity (43).

Purified LPL and variants, $LPL_{HL\ lid}$ or $LPL_{HL\ helix}$, were assayed for nANGPTL4 inhibition by measuring the rate of substrate hydrolysis in the presence of increasing concentrations of nANGPTL4. Although LPL was sensitive to nANGPTL4 inhibition with a K_i of 1.7 ± 0.74 μM, both LPL_{HL} chimeric mutants appeared to be resistant to nANGPTL4 inhibition (Table 1). The $LPL_{HL\ helix}$ had a slight sensitivity to nANGPTL4 with an estimated K_i of 15 ± 7.0 μM (Fig. 4*C*). Unless 50% enzyme inhibition occurred, the reported K_i values could only be estimated. $LPL_{HL\ lid}$ showed a similar resistance to nANGPTL4 inhibition as HL, such that a K_i value could not be calculated (Fig. 4, *B* and *D*). These data suggest that both the lid and lid-proximal helix are necessary for nANGPTL4 binding LPL. Although it is possible that the mutations altered the three-dimensional struc-

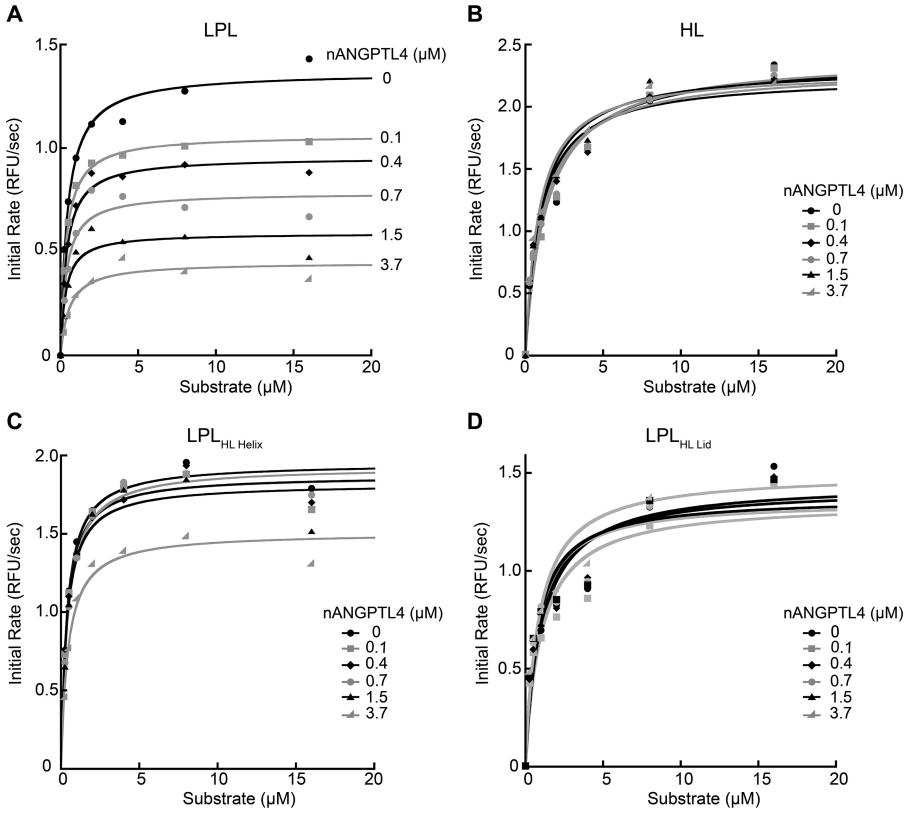

Figure 4. LPL_{HL} chimeric mutants are resistant to nANGPTL4 inhibition. Michaelis-Menten curves were generated in the presence of increasing concentrations of nANGPTL4 over multiple concentrations of fluorescent substrate to obtain K_i values. *A,* LPL is inhibited by nANGPTL4 with a K_i value of ~1.4 ± 0.13 μM. *B,* HL is resistant to nANGPTL4 inhibition. *C,* $LPL_{HL\ helix}$ is resistant to nANGPTL4 with an estimated K_i of 14.0 ± 1.4 μM. *D,* $LPL_{HL\ lid}$ is resistant to nANGPTL4, similar to HL; a K_i value could not be calculated. Representative data are shown of four biological replicates ± S.E. *RFU,* relative fluorescent units.

ture of the lipase, both LPL_{HL} chimeric molecules displayed no obvious catalytic defects (Table 1).

We next tested whether the furin protease cleavage region was necessary for nANGPTL4 inhibition (residues 288–309) (Fig. S3*A*). Furin protease recognizes the consensus sequence "R*XX*(K/R)" present in LPL at residues 294–297, resulting in inactive N- and C-terminal cleavage fragments (49, 50). In HL, the furin consensus sequence is disrupted by a proline residue and protected from proteolytic cleavage in this region (residues 314–334).

We first exchanged LPL residues 288–309 for the corresponding HL sequence (Fig. S3*A*). As expected, this mutation abolished furin cleavage in LPL but also abolished LPL enzymatic activity (Fig. S3, *B* and *C*). It is important to note that the proline residue in the corresponding HL sequence at position 294 may compromise the three-dimensional structure of LPL and possibly result in catalytic inactivation. Therefore, we split the full sequence into two parts: 288–299 and 300–309 (Fig. S3*A*). Similar to $LPL_{HL288-309}$, $LPL_{HL288-299}$ was not enzymatically active. Although $LPL_{HL300-309}$ does not contain the R294P mutation, its enzymatic activity could not be detected either (Fig. S3*B*). Western blot analysis revealed that nearly the entire population of $LPL_{HL300-309}$ was cleaved by furin protease (Fig. S3*C*) (49). Because we were unable to measure lipase activity for any of the LPL_{HL} furin cleavage chimeras, we cannot determine whether residues 288–309 are directly involved in nANGPTL4 binding.

Human HL_{LPL} chimeric proteins are sensitive to inhibition by nANGPTL4

To further validate sequences needed for nANGPTL4 inhibition of LPL, we aimed to "sensitize" HL to nANGPTL4 inhibition by generating human HL chimeric mutants containing the corresponding LPL sequences for the lid-proximal helix and the lid (Fig. 3). Similar to LPL_{HL} chimeric mutants, all HL_{LPL} chimeric mutants were generated using overlap extension PCR, whereby each sequence of interest was exchanged for the corresponding LPL sequence (Fig. 3).

$HL_{LPL\ lid}$ and $HL_{LPL\ helix}$ were kinetically similar to HL with average V_{max} and K_m values of 2.0 μmol/s and 0.6 μM, respectively, using the DGGR lipase substrate (Table 1). However, unlike HL, $HL_{LPL\ helix}$ and $HL_{LPL\ lid}$ were sensitive to nANGPTL4 inhibition with an estimated K_i of 32.7 ± 5.6 and 45.5 ± 2.4 μM, respectively (Fig. 5, *B* and *C*). $HL_{LPL\ lid\ +\ helix}$ appeared to be the most sensitive to inhibition with an estimated K_i of 22 ± 8.7 μM (Fig. 5*D*). Taken together, these data show that the LPL lid and the lid-proximal helix provide binding sites for nANGPTL4.

LPL lid peptide blocks nANGPTL4-mediated inhibition of LPL

Given that mutating the LPL lid abolished nANGPTL4 inhibition, we wanted to know whether the LPL lid domain alone could compete with full-length LPL for binding nANGPTL4. Therefore, we synthesized a peptide composed of the LPL lid sequence (CNIGEAIRVIAERGLGDVDQLVKC). The native LPL lid was circularized via a disulfide bond between two cys-

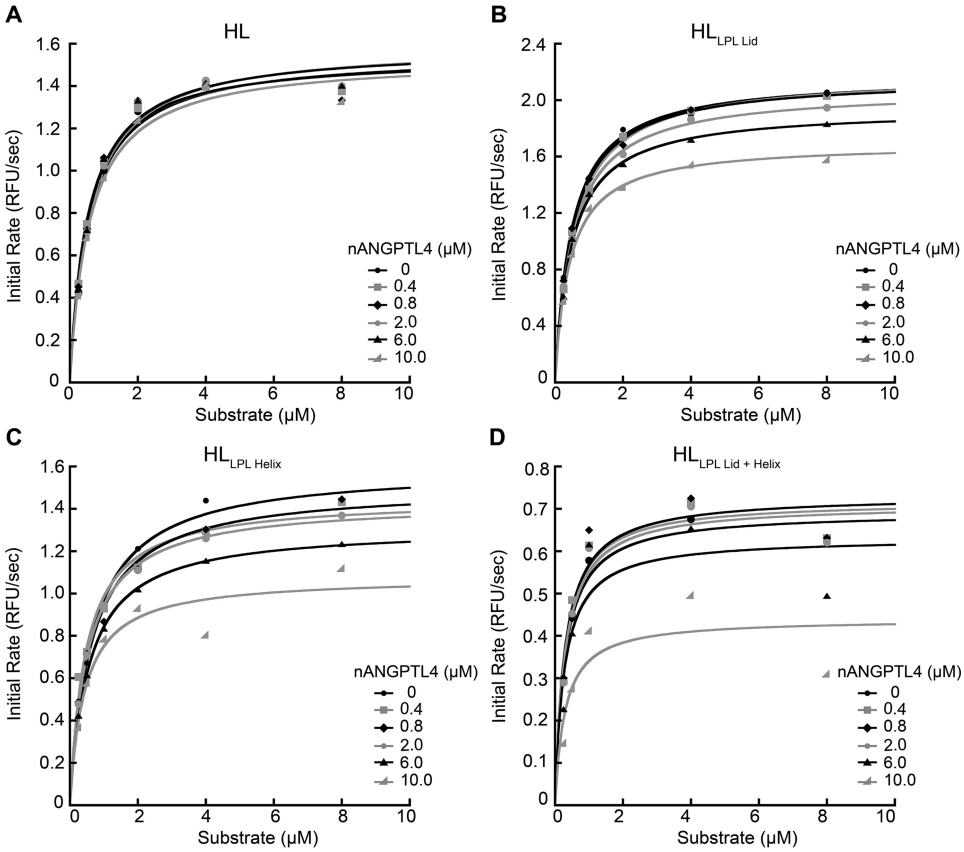

Figure 5. HL_{LPL} chimeric mutants are sensitive to nANGPTL4 inhibition. *A,* HL is resistant to nANGPTL4. *B,* $HL_{LPL\ lid}$ is slightly sensitive to nANGPTL4 inhibition with an estimated K_i of 42.9 ± 2.8 μM. *C,* $HL_{LPL\ helix}$ is moderately sensitized to inhibition with an estimated K_i of 30.3 ± 3.5 μM. *D,* $HL_{LPL\ lid\ +\ helix}$ is the most sensitive to inhibition an estimated K_i of 22.9 ± 5.3 μM. Representative data are shown of four biological replicates ± S.E. *RFU,* relative fluorescent units.

Table 1

Enzyme kinetics for each LPL and HL chimeric variant

Michaelis-Menten curves were generated for each lipase in the presence of increasing concentrations of nANGPTL4 over multiple fluorescent substrate concentrations. LPL and LPL_{HL} chimeric mutants have similar V_{max} and K_m values. $LPL_{HL\ lid}$ and $LPL_{HL\ helix}$ have an increased resistance to nANGPTL4 inhibition, relative to LPL. HL and HL_{LPL} chimeric mutants have similar V_{max} and K_m values, except $HL_{LPL\ lid\ +\ helix}$ has a significantly lower V_{max} than HL. HL_{LPL} chimeric mutants have increased sensitivity to nANGPTL4, relative to HL. Average values of at least three biological replicates ± S.D. RFU indicates relative fluorescent units.

Lipase	V_{max}	K_m	K_i
	RFU/s	*μM*	*μM*
LPL	1.19 ± 0.26	0.39 ± 0.04	1.71 ± 0.74
$LPL_{HL\ lid}$	1.78 ± 0.30	0.93 ± 0.28	
$LPL_{HL\ helix}$	1.80 ± 0.39	0.48 ± 0.07	15.11 ± 7.00
HL	1.91 ± 0.57	0.91 ± 0.37	
$HL_{LPL\ lid}$	2.10 ± 0.39	0.57 ± 0.08	45.52 ± 2.37
$HL_{LPL\ helix}$	1.45 ± 0.17	0.61 ± 0.05	32.70 ± 5.61
$HL_{LPL\ lid\ +\ helix}$	0.64 ± 0.03	0.43 ± 0.10	22.00 ± 8.72

teine residues at the termini of the lid motif. The synthetic lid peptide was tested in cyclic form (disulfide-bonded) or linear form (NEM-capped). Correct synthesis and circularization of the peptide were verified by MS, as shown in Fig. S4, *A* and *B*. We tested whether the peptide could prevent LPL inhibition by nANGPTL4 by incubating the inhibition reaction with increasing concentrations of either cyclic and linear NEM-capped lid peptide. Interestingly, the cyclic peptide protected full-length LPL from nANGPTL4 inhibition in a dose-dependent manner, whereas the linear NEM-capped peptide did not (Fig. 6, *A* and *B*). Presumably, the cyclic peptide adopts a structure similar to the native lid domain. Isothermal titration calorimetry (ITC) was used to confirm that the cyclic lid peptide binds nANGPTL4 with micromolar affinity. These data suggest that two lid peptides bind each nANGPTL4 tetramer with a K_d of ~57 μM (Fig. 6*C*). Although the ITC shows that the lid peptide binds nANGPTL4 with relatively low affinity, these data confirm that the LPL lid is an important site for nANGPTL4 binding.

Discussion

Hypertriglyceridemia is an independent risk factor for cardiovascular disease with relatively limited treatment options and, therefore, an unmet need for new therapies (6, 10). Given LPL has a direct influence on plasma triglyceride levels, it is a promising target for novel triglyceride-lowering therapeutics. One approach for targeting LPL is to prevent its inhibition by ANGPTL4. Previous reports describing ANGPTL4 knockout animals demonstrated significantly reduced triglyceride levels with little negative side effects under standard chow diets (25, 27). However, the safety of ANGPTL4 knockdown has been called into question due to severe lymphadenopathy observed in animals placed on high-fat diets (27, 28). Intriguingly, humans with loss-of-function mutations in ANGPTL4 do not appear to be at an increased risk for lymphadenopathy (25, 26). Therefore, additional research is needed to assess whether specifically blocking ANGPTL4 inhibition of LPL can be a viable treatment for hypertriglyceridemia. Our goal was to study the interaction of nANGPTL4 with LPL to inform the development of specific inhibitors for this interaction.

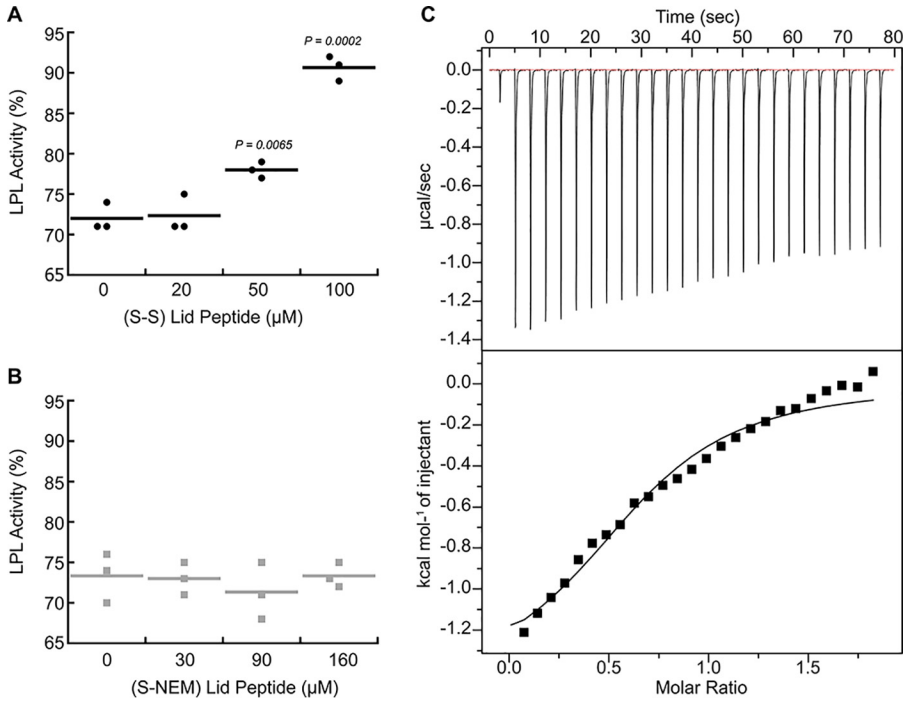

Figure 6. LPL lid mimetic binds nANGPTL4 and prevents inhibition of full-length LPL. *A,* cyclic lid peptide (S-S) blocks nANGPTL4 inhibition of full-length LPL in a dose-dependent manner. *B,* linear lid peptide with terminal cysteine residues capped with NEM does not block nANGPTL4 inhibition. *C,* isothermal titration calorimetry reveals the cyclic lid peptide binds nANGPTL4 with an approximate $K_d = 57\ \mu M$. Stoichiometry (*n* value) was calculated as two peptides binding every one ANGPTL4 tetramer. Representative data are shown of three biological replicates.

The exact mechanism for LPL inhibition by ANGPTL4 has been controversial. nANGPTL4 was first shown to irreversibly inhibit LPL by converting active dimers into inactive monomers (52, 53). Our previous data support an alternative model, whereby nANGPTL4 inhibits LPL in a reversible, noncompetitive mechanism (54, 55). The difference in observed mechanisms of inhibition may depend on the initial stability of the LPL in the assay. Purified LPL is notoriously unstable in standard buffer conditions and is prone to thermal denaturation (54). Therefore, many *in vitro* LPL activity assays and purification protocols use a bile acid, deoxycholate, to stabilize LPL (40, 50, 54–58). In the presence of deoxycholate, nANGPTL4 inhibits LPL by a reversible, noncompetitive mechanism (40, 54). Because LPL is known to have enhanced thermal stability within the biological fluids that contain bile acids, like serum and milk, we used them to better mimic physiological conditions in our kinetic assays (58, 59).

We have identified both the lid and lid-proximal helix as key nANGPTL4-binding sites. Removing these sites from LPL abolished nANGPTL4 binding and protected the enzyme from inhibition. Alternatively, cloning these sites into HL sensitized this resistant lipase to nANGPTL4 inhibition. Our data suggest nANGPTL4 binds the lid and lid-proximal region of LPL, which may prevent proper lid function and inhibit substrate catalysis. There are conflicting reports whether nANGPTL4 can inhibit LPL in the presence of natural chylomicron or very LDL substrates (58, 60). Here, the synthetic substrate DGGR was needed to enable precise measurements of LPL inhibition kinetics. Natural lipoprotein substrates have different properties than DGGR, so our work does not address this conflict.

Our HDX-MS data also identified a third potential binding site for nANGPTL4 on LPL at residues surrounding its furin cleavage site (residues 288–309). LPL is inactivated by furin protease cleavage into the N- and C-terminal domains at the consensus sequence "RAKR" (residues 294–297). Although we were unable to generate enzymatically active chimeric mutants at this site, we have shown that furin-resistant LPL point mutants, R297N and R297N/S298C, are sensitive to nANGPTL4 inhibition (50). These data suggest residues Arg-297 and Ser-298 may not be necessary for nANGPTL4-mediated inhibition of LPL. Recent reports have shown that ANGPTL4 enhances furin cleavage of LPL in adipocytes (49). Given that ANGPTL4 is also cleaved by the furin protease, it is possible that ANGPTL4 binds LPL intracellularly to recruit the furin protease for cleavage of both ANGPTL4 and LPL.

Finally, we demonstrate that a small peptide containing the LPL lid sequence can protect full-length LPL from nANGPTL4 inhibition. Although this interaction is not yet sufficiently strong, it serves as a starting point for development of potent peptide inhibitors for nANGPTL4 that specifically abolish LPL inhibition and leave both full-length and cleaved forms of ANGPTL4 intact to perform their other functions.

Experimental procedures

Molecular cloning

Human LPL, HL, and chimeric mutants were cloned into pCDNA5/FRT/TO vectors (ThermoFisher Scientific) containing lipase maturation factor 1 (LMF1) with an internal ribosome entry site (IRES) for co-expression. All constructs contain a 6× polyhistidine-tag on the C terminus, except the WT HL

construct has no tag. All chimeric mutants were generated using overlap extension PCR. Cloning of pET16B nANGPTL4 was previously described (54). All plasmid sequences are available upon request.

Cell culture and protein expression

LPL, HL, and chimeric mutant plasmids were stably integrated into FlpIn™ T-REx™ HEK293 cell lines (ThermoFisher Scientific) using the manufacturer's instructions. Each stable cell line was maintained in Dulbecco's modified Eagle's medium, 10% fetal bovine serum, 1% penicillin/streptomycin, and 1% L-glutamine (growth media). At 70% confluence, cells were given Dulbecco's modified Eagle's medium, 1% fetal bovine serum, 1% penicillin/streptomycin, 1% L-glutamine, 10 units/ml heparin, and 2 μg/ml tetracycline (expression media) to induce the expression of lipase. Expression media for all LPL species and HL was collected and flash-frozen in liquid nitrogen every 24 h for 6 days. Expression media for all HL variants was collected every 48 h, bound to nickel-Sepharose Excel™ resin (GE Healthcare), washed, and flash-frozen in liquid nitrogen for −80 °C storage until further purification as described below.

Protein purification

bLPL—bLPL was purified from fresh bovine milk as described previously (51). Briefly, chilled bovine milk was centrifuged and filtered using glass wool to remove milk fat. Solid NaCl was added to the skim milk to 0.34 mol/liter, and bLPL was purified using heparin-Sepharose 6 Fast Flow resin (GE Healthcare).

LPL, $LPL_{HL\ lid}$, and $LPL_{HL\ helix}$—Filtered expression media were loaded onto two tandem 1-ml HiTrap heparin-Sepharose high-performance columns (GE Healthcare) and then washed with 75 ml of 20 mM bis-tris, pH 6.5, 850 mM NaCl, 10% glycerol and eluted in 20 mM bis-tris, pH 6.5, 1500 mM NaCl, 10% glycerol over a linear gradient. All LPL-containing fractions were concentrated using Amicon ultracentrifugal units (Millipore), aliquoted, and flash-frozen for −80 °C storage until use.

HL—Filtered expression media loaded onto two tandem 1-ml HiTrap heparin-Sepharose high-performance columns (GE Healthcare) were washed with 20 ml of HL heparin buffer (20 mM Na_2HPO_4, pH 7.2, 500 mM NaCl, 10% glycerol) and eluted along a linear salt gradient from 500 to 2000 mM NaCl in HL heparin buffer. Fractions containing HL were pooled, concentrated using Amicon ultracentrifugal units (Millipore), aliquoted, and flash-frozen for −80 °C storage until use.

$HL_{LPL\ lid}$, $HL_{LPL\ helix}$, and $HL_{LPL\ lid\ +\ helix}$—Fresh expression media (150 ml) bound to nickel-Sepharose Excel™ resin (0.15 ml) (GE Healthcare) was washed with 2.5 ml using 20 mM Na_2HPO_4, pH 7.2, 360 mM NaCl, 10 mM imidazole, 10% glycerol. The resin was suspended in a high-salt storage buffer (1× PBS, 800 mM NaCl, 40% glycerol) and flash-frozen for storage at −80 °C until final purification. Frozen resin (1 ml total) was thawed on ice, washed with 10 ml of 20 mM Na_2HPO_4, pH 7.2, 500 mM NaCl, 50 mM imidazole, 10% glycerol, and eluted over 10 ml using 20 mM Na_2HPO_4, pH 7.2, 500 mM NaCl, 280 mM imidazole, 10% glycerol. Fractions containing HL chimeras were pooled and concentrated using dialysis against 400 g/liter high molecular weight polyethylene glycol in 20 mM bis-tris, pH 6.5. Concentrated samples were aliquoted and flash-frozen for storage at −80 °C until use.

nANGPTL4—His-GST–tagged nANGPTL4 was expressed in BL21 (DE3) cells, grown at 37 °C until reaching an A_{600} of 0.4, and induced with 0.1 mM isopropyl 1-thio-β-D-galactopyranoside for 16 h at 18 °C. Cells were pelleted at 6000 × *g*, resuspended in 20 mM Tris, pH 8.3, 360 mM NaCl, 20 mM imidazole, 1 mM betaine, 1 mM fresh phenylmethylsulfonyl fluoride (Sigma), and lysed using Emulisflex C5 (Avestin) at 15,000 p.s.i. Lysate was cleared by centrifugation at 34,000 × *g* for 60 min. Cleared lysate was added to equilibrated nickel-nitrilotriacetic acid resin (Qiagen). Resin was washed with 10 column volumes using 20 mM Tris, pH 8.3, 360 mM NaCl, 80 mM imidazole, 1 mM betaine, followed by a second wash using 20 mM Tris, pH 8.3, 150 mM NaCl, 80 mM imidazole, 1 mM betaine. His-GST-nANGPTL4 was eluted over 10 column volumes using 20 mM Tris, pH 8.3, 150 mM NaCl, 500 mM imidazole, 1 mM betaine. Elution fractions containing His-GST-nANGPTL4 were combined with 32 μg/ml tobacco etch virus, 3 mM reduced glutathione (GSH), and 0.3 mM oxidized GSH (GSSG) for cleavage of the N-terminal His-GST tag. Protein fractions were dialyzed into Mono S start buffer (20 mM Tris, pH 8.3, 100 mM NaCl), injected onto a 1-ml Mono S 5/50 GL column (GE Healthcare), and eluted over a linear gradient from 100 to 2000 mM NaCl in Mono S buffer. Fractions containing nANGPTL4 were furthered purified using HiLoad™ 16/600 Superdex™ 200 PG (GE Healthcare) in nANGPTL4 storage buffer (20 mM Tris, pH 8.3, 150 mM NaCl, 5% glycerol). Fractions containing nANGPTL4 were concentrated using Amicon ultracentrifugal units (Millipore), aliquoted, and flash-frozen for −80 °C storage until use.

Quantification of active lipase

Quantification was performed as described previously (55). Briefly, ActivX™ TAMRA-FP serine hydrolase probe (ThermoFisher Scientific) was used to label active LPL and HL variants where bovine LPL of known concentration was used as a protein standard. The relative purity of all purified protein can be seen by both Coomassie stain and TAMRA-FP labeling in Fig. S5, *A–D*.

HDX-MS

HDX labeling—bLPL and nANGPTL4 alone were diluted in 50 mM sodium phosphate buffer, pH 7.2, to 8 and 16 μM, respectively, and a condition with 8 μM bLPL and 16 μM nANGPTL4 was created prior to deuterium labeling. An automated HDX labeling LEAP robot was used for deuterium labeling. Briefly, 5 μl of each protein sample were diluted with 45 μl of 50 mM sodium phosphate in H_2O for time 0 injections or 45 μl of 50 mM sodium phosphate in D_2O (99.9% Sigma) for deuterium uptake injections at 1, 5, and 10 min. Deuterium exchange was quenched with 45 μl of pre-chilled 0.3% formic acid in water with 1 mM TCEP at the corresponding times. Quenched samples were subjected to on-line pepsin digestion using Waters Enzymate BEH pepsin column (2.1 × 30 mm × 5 μm) at 200 μl/min at 20 °C for 2 min (pH 2.5, 0.05% formic acid in water). Sample processing was managed within Waters HDX Acquity Module (Waters).

LC–MS-MS—Downstream LC–MS-MS was acquired in duplicate using the nanoAcquity UPLC system (Waters) coupled to a Waters Synapt G2 high-resolution accurate mass tandem mass spectrometer via an electrospray ionization source. The sample was first trapped on a VanGuard 2.1 × 5-mm BEH C18 1.7-μm trapping column (40 μl/min at 5% v/v water/acetonitrile, 0.1% formic acid). Analytical separation was performed using a 1.7-μm Acquity BEH130 C18 1 × 100-mm column (Waters Corp.) using a linear gradient from 5% acetonitrile, 0.1% formic acid to 35% acetonitrile, 0.1% formic acid over 7 min at 40 μl/min. Trapping and analytical separation were all performed at 1.0 °C with the HDX manager. Data collection on the Synapt G2 mass spectrometer was performed in an ion-mobility enabled data-independent acquisition mode of acquisition alternating between a 1.0-s low energy scan from m/z 50 to 2000 followed by a 1.0-s high energy scan from m/z 50 to 2000. Every 30 s, a low energy lock-mass scan of 400 fmol/μl Glu-Fibronectin peptide was performed.

Data analysis—All nondeuterated, time 0, data files were imported and searched within ProteinLynx Global Server (version 2.5.2) against a SwissProt_Human database containing bLPL and ANGPTL4 sequences. Nonspecific enzyme rules were selected with ±10 ppm mass accuracy tolerances and 5% retention time relative standard deviation criteria. ProteinLynx Global Server peptide score of at least 6.5 was included in the final analysis for a final peptide false discovery rate of < 2.0%. DynamX HDX Data Analysis Software (version 2.0, Waters) was used to calculate deuterium uptake for all identified peptide sequences. To identify residues of differential uptake on bLPL as a function of nANGPTL4, or vice versa, the calculated uptake values were subjected to an unpaired two-tailed Student's t test calculation at each time point for every condition. Only sites with significant differential uptake with a p value < 0.05 were selected for manual interrogation to ensure correct identification of peaks with no interference from neighboring peaks and to assess the global uptake distribution across all time points. Deuterium uptake was represented in a heat map using percent deuterium uptake values for all peptides with a standard deviation of less than 0.2 Da at each time point. Heat maps for bLPL alone and bLPL + nANGPTL4 were generated using 393 and 350 unique peptides, respectively. Heat maps for nANGPTL4 alone and nANGPTL4 + bLPL were generated using 520 and 505 unique peptides, respectively. All raw data used in our analysis can be found in Table S1.

Peptide production

Peptide synthesis was carried out using solid-phase peptide synthesis on a Biotage Initiator+ Alstra microwave peptide synthesizer using rink amide ChemMatrix resin (Biotage). Peptidic scaffolds were synthesized from the C to the N terminus with a C-terminal amide functional group using standard Fmoc (fluorenylmethoxycarbonyl) chemistry. The building blocks are composed of commercially available *N*-α-Fmoc–L-amino acids. Briefly, the resin was initially wetted and swollen with 1:1 mixture of dichloromethane and DMF. Fmoc deprotection was achieved using incubation of the resin with 20% (v/v) piperidine/DMF for 3 and 10 min each, with a DMF wash at the end of each incubation step. The *N*-α-Fmoc–L-amino acids (5 eq) were coupled using 1-[bis(dimethylamino)methylene]-1*H*-1,2,3-triazolo[4,5-b]pyridinium 3-oxide hexafluorophosphate (5 eq) as the coupling agent and diisopropylethylamine (10 eq) as the base. Coupling steps were carried out at 75 °C for 5 min each using microwave irradiation. After the final deprotection to obtain a primary amine at the N terminus of the synthesized peptide, the resin was washed with dichloromethane and dried. The synthesized peptide was cleaved from the resin using 94–95% (v/v) TFA, 2.5% (v/v) water, and 2.5% (v/v) triisopropylsilane while incubating at 37 °C for 1 h followed by incubation at room temperature for 30 min. Resin-cleaved peptide was precipitated by the dropwise addition of the cleavage reaction mixture into cold diethyl ether. The precipitate was separated by centrifugation, and the supernatant was decanted. Dried peptide was dissolved in DMSO and diluted with a mixture of 50% (v/v) acetonitrile/water. The crude peptide was then purified using semi-preparative HPLC. Each fraction was analyzed using the UV trace at 220 and 280 nm and LC-MS. Fractions containing pure peptide were collected and lyophilized. The solid peptide was dissolved in DMSO and then diluted to a peptide concentration of 200 μM using 0.1 M ammonium bicarbonate, pH 8.0. This step allowed it to circularize via intramolecular disulfide bond formation. Completion of circularization was verified by LC-MS, and the peptide was lyophilized and stored at −20 °C until used.

NEM capping of lid peptide—LPL lid peptide purified as described above was dissolved in DMSO and diluted to a final concentration of 0.4% DMSO and 0.1 M TCEP using 1× PBS, pH 7.8. The solution was incubated at 37 °C for 15 min to reduce disulfide bonds. Following TCEP reduction, 0.1 M NEM was added to the reaction and incubated at 37 °C for 60 min. The capped peptide was recovered by HPLC, verified by LC-MS, and lyophilized for storage at −20 °C.

Inhibition of LPL, HL, and chimeric mutants by nANGPTL4—Inhibition assays using purified lipase and lipase variants by nANGPTL4 were carried out essentially as described (2). LPL and bLPL are equivalently inhibited by nANGPTL4. Briefly, nANGPTL4 was added to dilute LPL, HL, or chimeric mutants at a final volume of 70 μl/reaction. The reaction was initiated by the addition of 30 μl of varying concentrations of fluorescent substrate DGGR (Sigma) in anzergent 3-16 (Affymetrix), to a final volume of 100 μl. Samples were shaken in a Spectramax M5 plate reader at 37 °C for 5 s, and substrate hydrolysis was measured by fluorescence excitation at 529 nM, emission at 600 nM, and a filter of 590 nm. Final assay buffer concentrations were 215 mM NaCl, 1 mM deoxycholate, 20 mM Tris, pH 8.0, 0.2% fatty acid–free BSA, and 0.01% anzergent 3-16. Final ANGPTL4 concentrations were 0, 0.2, 0.4, 0.8, 1.5, and 3.7 μM or 0, 0.4, 0.8, 2, 6, and 10 μM. The rate of initial lipase substrate hydrolysis was plotted as a function of substrate concentration. Next, data were fit to the equation for noncompetitive inhibition: $v = V_{max}\cdot[S]/\{(K_m\cdot(1 + [I]/K_i)) + ([S]\cdot(1 + [I]/K_i))\}$, where V_{max} is the uninhibited maximum rate of substrate hydrolysis; K_m is the K_m value; [S] is substrate concentration; [I] is inhibitor concentration; and K_i is the inhibition constant. Data were fit

using simultaneous nonlinear regression with the program Mathematica (Wolfram Research).

Inhibition of LPL by nANGPTL4 in the presence of an LPL lid peptide—LPL inhibition by nANGPTL4 was measured using the DGGR fluorescent assay described above in the presence of the LPL lid peptide. nANGPTL4 (0 or 0.4 μM) was incubated with increasing concentrations of cyclic lid peptide (0, 20, 50, or 100 μM) or linear NEM-capped peptide (0, 30, 90, or 160 μM) for 10 min at room temperature. After incubation, the mixture was added to dilute LPL in a final volume of 70 μl/reaction and incubated for an additional 5 min at room temperature. LPL activity was measured upon the addition of 30 μl of DGGR for a final reaction volume of 100 μl. Final assay buffer concentrations were 20 mM Tris, pH 8.0, 150 mM NaCl, 1 mM deoxycholate, 0.2% fatty-acid free BSA, 0.01% anzergent 3-16, 10 μM DGGR, 0.8% DMSO, 2.5 nM LPL, 0 or 0.4 μM nANGPTL4, and 0, 20, 50, or 100 μM cyclic lid peptide or 0, 30, 90, 160 μM linear NEM-capped peptide.

Isothermal titration calorimetry—Lyophilized lid peptide was resuspended in DMSO and diluted in nANGPTL4 dialysis buffer (1× PBS, pH 7.8) to a final concentration of 3087 μM and 4% DMSO. Purified nANGPTL4 was at a concentration of 338 μM and brought to 4% DMSO to exactly match the peptide buffer. Isothermal titrations were performed using the MicroCal Auto-iTC200 (Malvern Panalytical). Injections of 1.5 μl of peptide were added in 180-s intervals at 10 °C. Heat of dilution was measured by titrating the peptide into a blank solution and subtracted from our data before a one-site curve fitting was performed using MicroCal Auto-iTC200 software. Stoichiometry (N), association, and dissociation constants (K_a and K_d) and enthalpy change (ΔH) were obtained directly from the data.

Author contributions—A. R. G. and S. B. N. conceptualization; A. R. G. and S. V. G. data curation; A. R. G. and S. V. G. formal analysis; A. A. B. and S. B. N. supervision; A. A. B. and S. B. N. funding acquisition; A. R. G. and S. V. G. investigation; A. R. G., S. V. G., A. A. B., and S. B. N. methodology; A. R. G. and S. V. G. writing-original draft; A. R. G., S. V. G., A. A. B., and S. B. N. writing-review and editing.

Acknowledgments—We thank Duke University School of Medicine for the use of Proteomics and Metabolomics Shared Resource, particularly Dr. Erik Soderblom, who provided expertise in hydrogen–deuterium exchange MS. We also thank Benjamin Keith for assistance with heat map generation and Michael Lafferty for design and construction of the $LPL_{HL\ lid}$ chimera.

References

1. Mead, J. R., Irvine, S. A., and Ramji, D. P. (2002) Lipoprotein lipase: structure, function, regulation, and role in disease. *J. Mol. Med.* **80,** 753–769 CrossRef Medline
2. Dallinga-Thie, G. M., Kroon, J., Borén, J., and Chapman, M. J. (2016) Triglyceride-rich lipoproteins and remnants: targets for therapy? *Curr. Cardiol. Rep.* **18,** 67 CrossRef Medline
3. Santamarina-Fojo, S., and Brewer, H. B., Jr. (1994) Lipoprotein lipase: structure, function and mechanism of action. *Int. J. Clin. Lab. Res.* **24,** 143–147 CrossRef Medline
4. Goldberg, I. J. (1996) Lipoprotein lipase and lipolysis: central roles in lipoprotein metabolism and atherogenesis. *J. Lipid Res.* **37,** 693–707 Medline
5. Brahm, A. J., and Hegele, R. A. (2015) Chylomicronaemia–current diagnosis and future therapies. *Nat. Rev. Endocrinol.* **11,** 352–362 CrossRef Medline
6. Yuan, G., Al-Shali, K. Z., and Hegele, R. A. (2007) Hypertriglyceridemia: its etiology, effects and treatment. *CMAJ.* **176,** 1113–1120 CrossRef Medline
7. Karalis, D. G. (2017) A review of clinical practice guidelines for the management of hypertriglyceridemia: a focus on high dose omega-3 fatty acids. *Adv. Ther.* **34,** 300–323 CrossRef Medline
8. Rader, D. J. (2016) New therapeutic approaches to the treatment of dyslipidemia. *Cell Metab.* **23,** 405–412 CrossRef Medline
9. Sniderman, A. D., Couture, P., Martin, S. S., DeGraaf, J., Lawler, P. R., Cromwell, W. C., Wilkins, J. T., and Thanassoulis, G. (2018) Hypertriglyceridemia and cardiovascular risk: a cautionary note about metabolic confounding. *J. Lipid Res.* **59,** 1266–1275 CrossRef Medline
10. Tenenbaum, A., Klempfner, R., and Fisman, E. Z. (2014) Hypertriglyceridemia: a too long unfairly neglected major cardiovascular risk factor. *Cardiovasc. Diabetol.* **13,** 159 CrossRef Medline
11. Peng, J., Luo, F., Ruan, G., Peng, R., and Li, X. (2017) Hypertriglyceridemia and atherosclerosis. *Lipids Health Dis.* **16,** 233 CrossRef Medline
12. Sandoval, J. C., Nakagawa-Toyama, Y., Masuda, D., Tochino, Y., Nakaoka, H., Kawase, R., Yuasa-Kawase, M., Nakatani, K., Inagaki, M., Tsubakio-Yamamoto, K., Ohama, T., Matsuyama, A., Nishida, M., Ishigami, M., Komuro, I., and Yamashita, S. (2010) Molecular mechanisms of ezetimibe-induced attenuation of postprandial hypertriglyceridemia. *J. Atheroscler. Thromb.* **17,** 914–924 CrossRef Medline
13. Li, Y., He, P.-P., Zhang, D.-W., Zheng, X.-L., Cayabyab, F. S., Yin, W.-D., and Tang, C.-K. (2014) Lipoprotein lipase: from gene to atherosclerosis. *Atherosclerosis* **237,** 597–608 CrossRef Medline
14. Karpe, F., Olivecrona, T., Olivecrona, G., Samra, J. S., Summers, L. K., Humphreys, S. M., and Frayn, K. N. (1998) Lipoprotein lipase transport in plasma: role of muscle and adipose tissues in regulation of plasma lipoprotein lipase concentrations. *J. Lipid Res.* **39,** 2387–2393 Medline
15. Zhang, R. (2016) The ANGPTL3–4-8 model, a molecular mechanism for triglyceride trafficking. *Open Biol.* **6,** 150272 CrossRef Medline
16. Bergö, M., Olivecrona, G., and Olivecrona, T. (1996) Forms of lipoprotein lipase in rat tissues: in adipose tissue the proportion of inactive lipase increases on fasting. *Biochem. J.* **313,** 893–898 CrossRef Medline
17. Li, Y., and Teng, C. (2014) Angiopoietin-like proteins 3, 4 and 8: regulating lipid metabolism and providing new hope for metabolic syndrome. *J. Drug Target* **22,** 679–687 CrossRef Medline
18. Dijk, W., and Kersten, S. (2014) Regulation of lipoprotein lipase by Angptl4. *Trends Endocrinol. Metab.* **25,** 146–155 CrossRef Medline
19. Romeo, S., Pennacchio, L. A., Fu, Y., Boerwinkle, E., Tybjaerg-Hansen, A., Hobbs, H. H., and Cohen, J. C. (2007) Population-based resequencing of ANGPTL4 uncovers variations that reduce triglycerides and increase HDL. *Nat. Genet.* **39,** 513–516 CrossRef Medline
20. Myocardial Infarction Genetics and CARDIoGRAM Exome Consortia Investigators, Stitziel, N. O., Stirrups, K. E., Masca, N. G., Erdmann, J., Ferrario, P. G., König, I. R., Weeke, P. E., Webb, T. R., Auer, P. L., Schick, U. M., Lu, Y., Zhang, H., Dube, M. P., Goel, A., et al. (2016) Coding variation in ANGPTL4, LPL, and SVEP1 and the risk of coronary disease. *N. Engl. J. Med.* **374,** 1134–1144 CrossRef Medline
21. Kathiresan, S., Willer, C. J., Peloso, G. M., Demissie, S., Musunuru, K., Schadt, E. E., Kaplan, L., Bennett, D., Li, Y., Tanaka, T., Voight, B. F., Bonnycastle, L. L., Jackson, A. U., Crawford, G., Surti, A., *et al.* (2009) Common variants at 30 loci contribute to polygenic dyslipidemia. *Nat. Genet.* **41,** 56–65 CrossRef Medline
22. Noto, D., Arca, M., Tarugi, P., Cefalù, A. B., Barbagallo, C. M., and Averna, M. R. (2017) Association between familial hypobetalipoproteinemia and the risk of diabetes. Is this the other side of the cholesterol–diabetes connection? A systematic review of literature. *Acta Diabetol.* **54,** 111–122 CrossRef Medline
23. Stitziel, N. O., Khera, A. V., Wang, X., Bierhals, A. J., Vourakis, A. C., Sperry, A. E., Natarajan, P., Klarin, D., Emdin, C. A., Zekavat, S. M., Nomura, A., Erdmann, J., Schunkert, H., Samani, N. J., Kraus, W. E., *et al.* (2017) ANGPTL3 deficiency and protection against coronary artery disease. *J. Am. Coll. Cardiol.* **69,** 2054–2063 CrossRef Medline

24. Graham, M. J., Lee, R. G., Brandt, T. A., Tai, L.-J., Fu, W., Peralta, R., Yu, R., Hurh, E., Paz, E., McEvoy, B. W., Baker, B. F., Pham, N. C., Digenio, A., Hughes, S. G., Geary, R. S., *et al.* (2017) Cardiovascular and metabolic effects of *ANGPTL3* antisense oligonucleotides. *N. Engl. J. Med.* **377,** 222–232 CrossRef Medline
25. Dewey, F. E., Gusarova, V., O'Dushlaine, C., Gottesman, O., Trejos, J., Hunt, C., Van Hout, C. V., Habegger, L., Buckler, D., Lai, K.-M., Leader, J. B., Murray, M. F., Ritchie, M. D., Kirchner, H. L., Ledbetter, D. H., *et al.* (2016) Inactivating variants in *ANGPTL4* and risk of coronary artery disease. *N. Engl. J. Med.* **374,** 1123–1133 CrossRef Medline
26. Gusarova, V., O'Dushlaine, C., Teslovich, T. M., Benotti, P. N., Mirshahi, T., Gottesman, O., Van Hout, C. V., Murray, M. F., Mahajan, A., Nielsen, J. B., Fritsche, L., Wulff, A. B., Gudbjartsson, D. F., Sjögren, M., Emdin, C. A., *et al.* (2018) Genetic inactivation of ANGPTL4 improves glucose homeostasis and is associated with reduced risk of diabetes. *Nat. Commun.* **9,** 2252 CrossRef Medline
27. Desai, U., Lee, E. C., Chung, K., Gao, C., Gay, J., Key, B., Hansen, G., Machajewski, D., Platt, K. A., Sands, A. T., Schneider, M., Van Sligtenhorst, I., Suwanichkul, A., Vogel, P., Wilganowski, N., *et al.* (2007) Lipid-lowering effects of anti-angiopoietin-like 4 antibody recapitulate the lipid phenotype found in angiopoietin-like 4 knockout mice. *Proc. Natl. Acad. Sci. U.S.A.* **104,** 11766–11771 CrossRef Medline
28. Lichtenstein, L., Mattijssen, F., de Wit, N. J., Georgiadi, A., Hooiveld, G. J., van der Meer, R., He, Y., Qi, L., Köster, A., Tamsma, J. T., Tan, N. S., Müller, M., and Kersten, S. (2010) Angptl4 protects against severe proinflammatory effects of saturated fat by inhibiting fatty acid uptake into mesenteric lymph node macrophages. *Cell Metab.* **12,** 580–592 CrossRef Medline
29. Zhu, P., Goh, Y. Y., Chin, H. F., Kersten, S., and Tan, N. S. (2012) Angiopoietin-like 4: a decade of research. *Biosci. Rep.* **32,** 211–219 CrossRef Medline
30. Yin, W., Romeo, S., Chang, S., Grishin, N. V., Hobbs, H. H., and Cohen, J. C. (2009) Genetic variation in ANGPTL4 provides insights into protein processing and function. *J. Biol. Chem.* **284,** 13213–13222 CrossRef Medline
31. Biterova, E., Esmaeeli, M., Alanen, H. I., Saaranen, M., and Ruddock, L. W. (2018) Structures of Angptl3 and Angptl4, modulators of triglyceride levels and coronary artery disease. *Sci. Rep.* **8,** 6752 CrossRef Medline
32. Ge, H., Yang, G., Huang, L., Motola, D. L., Pourbahrami, T., and Li, C. (2004) Oligomerization and regulated proteolytic processing of angiopoietin-like protein 4. *J. Biol. Chem.* **279,** 2038–2045 CrossRef Medline
33. Miida, T., and Hirayama, S. (2010) Impacts of angiopoietin-like proteins on lipoprotein metabolism and cardiovascular events. *Curr. Opin. Lipidol.* **21,** 70–75 CrossRef Medline
34. Lee, E. C., Desai, U., Gololobov, G., Hong, S., Feng, X., Yu, X. C., Gay, J., Wilganowski, N., Gao, C., Du, L. L., Chen, J., Hu, Y., Zhao, S., Kirkpatrick, L., Schneider, M., *et al.* (2009) Identification of a new functional domain in angiopoietin-like 3 (ANGPTL3) and angiopoietin-like 4 (ANGPTL4) involved in binding and inhibition of lipoprotein lipase (LPL). *J. Biol. Chem.* **284,** 13735–13745 CrossRef Medline
35. Yau, M. H., Wang, Y., Lam, K. S., Zhang, J., Wu, D., and Xu, A. (2009) A highly conserved motif within the NH_2-terminal coiled-coil domain of angiopoietin-like protein 4 confers its inhibitory effects on lipoprotein lipase by disrupting the enzyme dimerization. *J. Biol. Chem.* **284,** 11942–11952 CrossRef Medline
36. Bäckhed, F., Crawford, P. A., O'Donnell, D., and Gordon, J. I. (2007) Postnatal lymphatic partitioning from the blood vasculature in the small intestine requires fasting-induced adipose factor. *Proc. Natl. Acad. Sci. U.S.A.* **104,** 606–611 CrossRef Medline
37. Vadas, O., Jenkins, M. L., Dornan, G. L., and Burke, J. E. (2017) Using hydrogen–deuterium exchange mass spectrometry to examine protein–membrane interactions. *Methods Enzymol.* **583,** 143–172 CrossRef Medline
38. Oganesyan, I., Lento, C., and Wilson, D. J. (2018) Contemporary hydrogen deuterium exchange mass spectrometry. *Methods* **144,** 27–42 CrossRef Medline
39. Hayne, C. K., Yumerefendi, H., Cao, L., Gauer, J. W., Lafferty, M. J., Kuhlman, B., Erie, D. A., and Neher, S. B. (2018) We FRET so you don't have to: new models of the lipoprotein lipase dimer. *Biochemistry* **57,** 241–254 CrossRef Medline
40. Mysling, S., Kristensen, K. K., Larsson, M., Kovrov, O., Bensadouen, A., Jørgensen, T. J., Olivecrona, G., Young, S. G., and Ploug, M. (2016) The angiopoietin-like protein ANGPTL4 catalyzes unfolding of the hydrolase domain in lipoprotein lipase and the endothelial membrane protein GPIHBP1 counteracts this unfolding. *Elife* **5,** e20958 CrossRef Medline
41. Fang, J., Rand, K. D., Beuning, P. J., and Engen, J. R. (2011) False EX1 signatures caused by sample carryover during HX MS analyses. *Int. J. Mass Spectrom.* **302,** 19–25 CrossRef Medline
42. Segel, I. (1993) *Enzyme Kinetics: Behavior and Analysis of Rapid Equilibrium and Steady-state Enzyme Systems*, pp. 125–136, Wiley, New York
43. Kearse, M., Moir, R., Wilson, A., Stones-Havas, S., Cheung, M., Sturrock, S., Buxton, S., Cooper, A., Markowitz, S., Duran, C., Thierer, T., Ashton, B., Meintjes, P., and Drummond, A. (2012) Geneious basic: an integrated and extendable desktop software platform for the organization and analysis of sequence data. *Bioinformatics* **28,** 1647–1649 CrossRef Medline
44. Lichtenstein, L., Berbée, J. F., van Dijk, S. J., van Dijk, K. W., Bensadoun, A., Kema, I. P., Voshol, P. J., Müller, M., Rensen, P. C., and Kersten, S. (2007) Angptl4 upregulates cholesterol synthesis in liver via inhibition of LPL- and HL-dependent hepatic cholesterol uptake. *Arterioscler. Thromb. Vasc. Biol.* **27,** 2420–2427 CrossRef Medline
45. Köster, A., Chao, Y. B., Mosior, M., Ford, A., Gonzalez-DeWhitt, P. A., Hale, J. E., Li, D., Qiu, Y., Fraser, C. C., Yang, D. D., Heuer, J. G., Jaskunas, S. R., and Eacho, P. (2005) Transgenic angiopoietin-like (Angptl)4 overexpression and targeted disruption of Angptl4 and Angptl3: regulation of triglyceride metabolism. *Endocrinology.* **146,** 4943–4950 CrossRef Medline
46. Griffon, N., Budreck, E. C., Long, C. J., Broedl, U. C., Marchadier, D. H., Glick, J. M., and Rader, D. J. (2006) Substrate specificity of lipoprotein lipase and endothelial lipase: studies of lid chimeras. *J. Lipid Res.* **47,** 1803–1811 CrossRef Medline
47. Davis, R. C., Wong, H., Nikazy, J., Wang, K., Han, Q., and Schotz, M. C. (1992) Chimeras of hepatic lipase and lipoprotein lipase. Domain localization of enzyme-specific properties. *J. Biol. Chem.* **267,** 21499–21504 Medline
48. Dugi, K. A., Dichek, H. L., and Santamarina-Fojo, S. (1995) Human hepatic and lipoprotein lipase: the loop covering the catalytic site mediates lipase substrate specificity. *J. Biol. Chem.* **270,** 25396–25401 CrossRef Medline
49. Dijk, W., Beigneux, A. P., Larsson, M., Bensadoun, A., Young, S. G., and Kersten, S. (2016) Angiopoietin-like 4 promotes intracellular degradation of lipoprotein lipase in adipocytes. *J. Lipid Res.* **57,** 1670–1683 CrossRef Medline
50. Wu, M. J., Wolska, A., Roberts, B. S., Pearson, E. M., Gutgsell, A. R., Remaley, A. T., and Neher, S. B. (2018) Co-expression of novel furin-resistant LPL variants with LMF1 enhances LPL secretion and activity. *J. Lipid Res.* **59,** 2456–2465 CrossRef Medline
51. Bengtsson-Olivecrona, G., and Olivecrona, T. (1991) Phospholipase activity of milk lipoprotein lipase. *Methods Enzymol.* **197,** 345–356 CrossRef Medline
52. Sukonina, V., Lookene, A., Olivecrona, T., and Olivecrona, G. (2006) Angiopoietin-like protein 4 converts lipoprotein lipase to inactive monomers and modulates lipase activity in adipose tissue. *Proc. Natl. Acad. Sci. U.S.A.* **103,** 17450–17455 CrossRef Medline
53. Shan, L., Yu, X. C., Liu, Z., Hu, Y., Sturgis, L. T., Miranda, M. L., and Liu, Q. (2009) The angiopoietin-like proteins ANGPTL3 and ANGPTL4 inhibit lipoprotein lipase activity through distinct mechanisms. *J. Biol. Chem.* **284,** 1419–1424 CrossRef Medline
54. Lafferty, M. J., Bradford, K. C., Erie, D. A., and Neher, S. B. (2013) Angiopoietin-like protein 4 inhibition of lipoprotein lipase: evidence for reversible complex formation. *J. Biol. Chem.* **288,** 28524–28534 CrossRef Medline
55. Hayne, C. K., Lafferty, M. J., Eglinger, B. J., Kane, J. P., and Neher, S. B. (2017) Biochemical analysis of the lipoprotein lipase truncation variant, LPL S447X, reveals increased lipoprotein uptake. *Biochemistry* **56,** 525–533 CrossRef Medline

56. Mysling, S., Kristensen, K. K., Larsson, M., Beigneux, A. P., Gårdsvoll, H., Fong, L. G., Bensadouen, A., Jørgensen, T. J., Young, S. G., and Ploug, M. (2016) The acidic domain of the endothelial membrane protein GPIHBP1 stabilizes lipoprotein lipase activity by preventing unfolding of its catalytic domain. *Elife* **5,** e12095 CrossRef Medline
57. Bengtsson, G., and Olivecrona, T. (1979) Binding of deoxycholate to lipoprotein lipase. *Biochim. Biophys. Acta* **575,** 471–474 CrossRef Medline
58. Reimund, M., Kovrov, O., Olivecrona, G., and Lookene, A. (2017) Lipoprotein lipase activity and interactions studied in human plasma by isothermal titration calorimetry. *J. Lipid Res.* **58,** 279–288 CrossRef Medline
59. Neville, M. C., Waxman, L. J., Jensen, D., and Eckel, R. H. (1991) Lipoprotein lipase in human milk: compartmentalization and effect of fasting, insulin, and glucose. *J. Lipid Res.* **32,** 251–257 Medline
60. Nilsson, S. K., Anderson, F., Ericsson, M., Larsson, M., Makoveichuk, E., Lookene, A., Heeren, J., and Olivecrona, G. (2012) Triacylglycerol-rich lipoproteins protect lipoprotein lipase from inactivation by ANGPTL3 and ANGPTL4. *Biochim. Biophys. Acta* **1821,** 1370–1378 CrossRef Medline